

Thesis Changes Log

Name of Candidate: Alexey P. Tsapenko

PhD Program: Physics (Optics)

Title of Thesis: Enhancing optoelectronic performance of randomly oriented single-walled carbon nanotube films

Supervisors: Prof. Albert Nasibulin, Skoltech, Russia

Prof. Esko Kauppinen, Aalto, Finland

Chair of PhD defense Jury: Prof. Nikolay Gippius, Skoltech *Email: N.Gippius@skoltech.ru*

Date of Thesis Defense: October 4, 2019

The thesis document includes the following changes in answer to the external review process.

Dear Jury Members,

Thanks a lot for your reviews with questions as well as comments and suggestions on how to improve my thesis.

Please find below both the detailed description of modifications made in the thesis final version and answers to the questions, comments. The pages in answers are mentioned according to the final version of the thesis.

Based on the Jury Member Report from *Professor Krizstian Kordas*, there have been made changes according to the following suggestions:

1. *“Grammar and phrasing shall be corrected”*

Answer:

Missing abbreviations and symbols, mistakes, phrasing, and misprints were corrected in the text.

2. *“2.1 Limited indium resources and increasing price of associated commodities should be mentioned.”*

Answer:

Section 2.1 was modified by mentioning the information along with the corresponding references. p.21 “In combination with the fact of being based on a rare-material as indium, resources of which are limited and the price of associated commodities is constantly increasing [11,12], ITO is extensively sought to be replaced with alternative materials.”

References:

- [11] S. Jewell, S.M. Kimball, Mineral Commodity Summaries, 2016. doi:10.3133/70202434.
[12] U.S. Geological Survey, MINERAL COMMODITY SUMMARIES 2019, 2019. doi:10.1007/978-3-540-47108-0-4.

3. *“2.3.1 CO2 as “catalyst stimulant”??? What do you mean by that? Etching the amorphous carbon from the surface of the Fe catalyst? Have you considered that inserting additional CO2 to the reaction gas of the disproportionation reaction will change (slow down) the reaction rate by reversing the process?”*

Answer:

Section 2.3.1 was modified with the appropriate terms and references to properly explain the observable effects during aerosol CVD synthesis. In addition to that, the effects of CO₂ introduction, including the increase of catalyst lifetime, was concisely explained.

p.23 “Because of plenty proven advantages, the aerosol CVD SWCNT synthesis technique was used for this work. Briefly, the synthesis is based on catalyst thermal decomposition and carbon monoxide (CO) disproportionation reaction on a catalyst particle surface. During this process, catalyst particle formation and subsequent growth of SWCNTs take place directly in the reactor flow (Figure 2.3.1-1). The reactor consists of a quartz tube placed in a furnace (hot zone), a precursor cartridge (filled with ferrocene/SiO₂ mixture) and a gas supply system (Figure 2.3.1-1). Catalyst precursor (ferrocene) vapor is delivered into the reactor hot zone by passing a gas stream (CO) through the pre-heated up to 60 °C cartridge. Additionally, the flow of CO and carbon dioxide (CO₂) mixture passes through the reactor. Here, CO₂ increases the catalyst lifetime as it preserves the catalyst from deactivation [22,23]. The addition of CO₂ helps to control the output parameters of produced SWCNTs (for instance, longer nanotubes can be yielded at long catalyst lifetimes) as well as other synthesis conditions. The typical synthesis temperature range is from 750 to 1100 °C. Therefore, after partial ferrocene decomposition and catalyst particle formation in the hot zone, the catalytic CO disproportionation takes place along with the decomposition of hydrocarbon and ferrocene, which eventually lead to the dissolution of carbon into nanoparticle (NP). As a result, this ends up with NP saturation by carbon and carbon layer formation on the catalyst particle surface (SWCNT are formed in case when catalyst particle size is less or equal to 5 nm, core shells – when the size is larger than that).”

References:

[22] Y. Liao, A. Hussain, P. Laiho, Q. Zhang, Y. Tian, N. Wei, E. Ding, S.A. Khan, N.N. Nguyen, S. Ahmad, E.I. Kauppinen, Tuning Geometry of SWCNTs by CO₂ in Floating Catalyst CVD for High-Performance Transparent Conductive Films, *Adv. Mater. Interfaces*. 5 (2018) 1801209. doi:10.1002/admi.201801209.

[23] A.S. Anisimov, A.G. Nasibulin, H. Jiang, P. Launois, J. Cambedouzou, S.D. Shandakov, E.I. Kauppinen, Mechanistic investigations of single-walled carbon nanotube synthesis by ferrocene vapor decomposition in carbon monoxide, *Carbon N. Y.* 48 (2010) 380–388. doi:10.1016/j.carbon.2009.09.040.

4. “Conclusions: “The lowest value of 40 Ω/sq at a wavelength of 550 nm is measured for SWCNT films doped with HAuCl₄ dissolved in ethanol.” The sentence is a kind of fragment as it is not important what the optical wavelength is when mentioning the sheet resistance. (Probably the optical transmittance was also to be mentioned in the sentence.) Please note that there are also some similar confusing sentences at other places in the manuscript.”

Answer:

Thank you for the comments. This sentence as well as several more (including corresponding figure captions) were rewritten to explicitly show the relation of the measured sheet resistance R_S and optical transmittance at 550 nm T_{550} to the most frequently used comparison parameter of TCFs – equivalent sheet resistance R_{90} .

p.73 “The second approach uses several model dopant solvents to experimentally evaluate the influence of their nature on the resulted optoelectronic performance of doped SWCNT films. From the dependence of R_{90} on the solvent boiling point and its relation to the dispersive component of Hansen solubility theory it is concluded that the most significant factor in the doping process is the solvent evaporation rate. As a consequence, the lowest value of $R_{90} = 40 \Omega/\square$ is measured for SWCNT films doped with HAuCl₄ dissolved in ethanol. For solvents with a higher boiling point, we optimized the overall film resistance by adjusting the temperature at which the doping is carried out. The samples produced in this work showed superior performance along with better stability values compared to the reported before.”

Based on the Jury Member Report from *Professor Nikolay Gippius*, there have been made changes according to the following suggestions:

1. “In Sec. 2.3.3 the calculations of the electronic properties of SWCNT using enhanced TB method with accounting for the excitonic effects are mentioned. It is not clear from the text whether the modification of the Coulomb potential in SWCNT compared to bulk materials was taken into account.”

Answer:

The related part of the Section 2.3.3 was improved accordingly.

p.26 “The ETB model is based on the calculation of excitonic wave functions by solving the Bethe-Salpeter equation within the TB model. The screening effect of the π -electrons in CNTs is included. The unscreened Coulomb potential between carbon π -orbitals is modelled by the Ohno potential [24,25], which realistically describes organic polymer systems.”

References:

[24] V. Perebeinos, J. Tersoff, P. Avouris, Scaling of Excitons in Carbon Nanotubes, Phys. Rev. Lett. 92 (2004) 257402. doi:10.1103/PhysRevLett.92.257402.

[25] J. Jiang, R. Saito, G.G. Samsonidze, A. Jorio, S.G. Chou, G. Dresselhaus, M.S. Dresselhaus, Chirality dependence of exciton effects in single-wall carbon nanotubes: Tight-binding model, Phys. Rev. B. 75 (2007) 035407. doi:10.1103/PhysRevB.75.035407.

Based on the Jury Member Report from *Assistant Professor Georgy Fedorov*, there have been made changes according to the following suggestions:

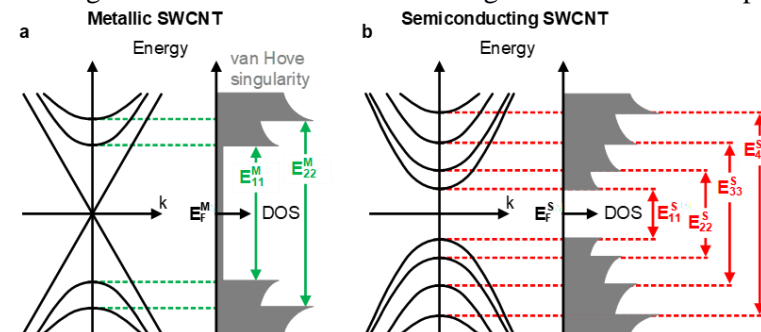
1. “CHAPTER 2

Figure 2.3.4-1. Electronic band structures and density of states (DOS) of (a) metallic and (b) semiconducting SWCNTs

Is misleading since it shows zero DOS for metallic CNT.”

Answer:

The Figure 2.3.4-1 was redrawn in the right manner and the capture was corrected.



p.27 “Figure 2.3.4-1. Illustration of the electronic band structures and density of states (DOS) of (a) metallic and (b) semiconducting SWCNTs.”

2. “The term “NHE” (Figure 2.3.4.3. caption) is never explained neither in text nor in the “List of abbreviations and symbols”

Answer:

The explanation of the missing abbreviation “NHE” was defined and incorporated into the “List of abbreviations and symbols” on p.14 and p.28 as well as in the Section 2.3.4 as discussed in the 3 question below.

p.27 “There are two main effects in the literature that govern doping [30–35]: electronegativity (in case of doping with atoms) and electrochemical potential (when doping with molecules). Both of them lead to the two main results of doping: a shift of E_F and an increase in the electron (n-doping) or hole (p-doping) carrier concentration. Additionally, the dopant may intercalate between SWCNT bundles and decrease the contact resistance between semiconducting and metallic nanotubes (reduction of the Schottky barrier height). Also, it is very important to estimate the position of E_F for a mixture of nanotubes in a film that has different DOS and consequently vHs.

Therefore, simply by knowing the electronegativity or electrochemical potential (E_{NHE}^j , where j stands for the SWCNT or dopant and NHE – for normal hydrogen electrode used to experimentally determine the potential) vs. distribution relations for nanotubes and the selected dopant, the doping process can be done with the depletion of energetic states related to the vHs, which in turn will lead to the disappearance of related peak in the absorbance spectrum and change in the work function (Figure 2.3.4-1 and Figure 2.3.4-2). To relate the work function (Φ) and electrochemical potential, the work function of SWCNTs is converted to the electrochemical potential value with the two equations: $E_{NHE}^{dopant} = \Phi/e - 4.44$ (describes the reduction potential of a molecular dopant, where E_{NHE}^{dopant} is the electrode potential of the dopant to the NHE and

4.44 V stands for absolute potential of the NHE in an aqueous solution at 295.05 K) and $E_{NHE}^{SWCNT} = a/d_t + b$ (describes the redox potential of the corresponding vHs of SWCNTs, where a and b are the fitting parameters and d_t is the diameter of a nanotube). For the experimental estimation of the redox potentials of SWCNTs, electrochemistry with photoluminescence and optical absorption spectroscopy are utilized [36,37]. Figure 2.3.4-2 illustrate the dependence of an electrochemical potential of SWCNTs on the chirality/diameters, where c_i and v_i are the corresponding conduction and valence bands of metallic (solid green) and semiconducting (solid red) nanotubes, E_F^j denotes the Fermi level of metallic “M” and semiconducting “S” nanotubes. By using these plots, the adsorption dopants are selected to engineer the work function of SWCNTs. Additionally, while there are quite many stable n-type dopants [38,39] (not shown in Figure 2.3.4-2), the issue is to find a comparable p-type one.”

References:

- [30] A. Murat, I. Rungger, C. Jin, S. Sanvito, U. Schwingenschlögl, Origin of the p-Type Character of AuCl₃ Functionalized Carbon Nanotubes, *J. Phys. Chem. C*. 118 (2014) 3319–3323. doi:10.1021/jp4100153.
- [31] S.M. Kim, K.K. Kim, Y.W. Jo, M.H. Park, S.J. Chae, D.L. Duong, K.I.M.E.T. Al, Role of Anions in the AuCl₃ -Doping of Carbon Nanotubes, *ACS Nano*. (2011) 1236–1242. doi:10.1021/nn1028532.
- [32] I.H. Lee, U.J. Kim, H. Bin Son, S.-M. Yoon, F. Yao, W.J. Yu, D.L. Duong, J.-Y. Choi, J.M. Kim, E.H. Lee, Y.H. Lee, Hygroscopic Effects on AuCl₃ -Doped Carbon Nanotubes, *J. Phys. Chem. C*. 114 (2010) 11618–11622. doi:10.1021/jp1036662.
- [33] K.K. Kim, J.J. Bae, H.K. Park, S.M. Kim, H.-Z. Geng, K.A. Park, H.-J. Shin, S.-M. Yoon, A. Benayad, J.-Y. Choi, Y.H. Lee, Fermi Level Engineering of Single-Walled Carbon Nanotubes by AuCl₃ Doping, *J. Am. Chem. Soc.* 130 (2008) 12757–12761. doi:10.1021/ja8038689.
- [34] S.M. Kim, K.K. Kim, D.L. Duong, Y. Hirana, Y. Tanaka, Y. Niidome, N. Nakashima, J. Kong, Y.H. Lee, Spectroscopic determination of the electrochemical potentials of n-type doped carbon nanotubes, *J. Phys. Chem. C*. 116 (2012) 5444–5449. doi:10.1021/jp211583t.
- [35] K.K. Kim, S.M. Kim, Y.H. Lee, Chemically Conjugated Carbon Nanotubes and Graphene for Carrier Modulation, *Acc. Chem. Res.* 49 (2016) 390–399. doi:10.1021/acs.accounts.5b00441.
- [36] Y. Tanaka, Y. Hirana, Y. Niidome, K. Kato, S. Saito, N. Nakashima, Experimentally determined redox potentials of individual (n,m) single-walled carbon nanotubes, *Angew. Chemie - Int. Ed.* (2009). doi:10.1002/anie.200902468.
- [37] D. Paolucci, M.M. Franco, M. Iurlò, M. Marcaccio, M. Prato, F. Zerbetto, A. Pénicaud, F. Paolucci, Singling out the electrochemistry of individual single-walled carbon nanotubes in solution, *J. Am. Chem. Soc.* (2008). doi:10.1021/ja710625p.
- [38] S.M. Kim, J.H. Jang, K.K. Kim, H.K. Park, J.J. Bae, W.J. Yu, H. Lee, G. Kim, D.D. Loc, U.J. Kim, E.H. Lee, H.J. Shin, J.Y. Choi, Y.H. Lee, Reduction-controlled viologen in bisolvent as an environmentally stable n-type dopant for carbon nanotubes, *J. Am. Chem. Soc.* (2009). doi:10.1021/ja807480g.
- [39] B.R. Kang, W.J. Yu, K.K. Kim, H.K. Park, S.M. Kim, Y. Park, C. Kim, H.J. Shin, U. Kim, E.H. Lee, J.Y. Choi, Y.H. Lee, Restorable type conversion of carbon nanotube transistor using pyrolytically controlled antioxidizing photosynthesis coenzyme, *Adv. Funct. Mater.* (2009). doi:10.1002/adfm.200801712.

3. “The effect of film doping is discussed poorly in the section 2.3.4 Figure 2.3.4.3 should be Figure 2.3.4.2. The term “absorption doping” probably should be replaced by “adsorption doping”

Answer:

The discussion on film doping was broadened. The Figure capture and its mentioning were revised. The appropriate term “adsorption doping” associated with the doping technique used during this work was corrected all over the thesis text.

p.28 “As previously discussed, the doping ability of various p-type dopants is closely related to the reduction potentials of the chemicals (their electrochemical potentials) they consist of. If the electrochemical potentials of SWCNTs are compared against the reduction potentials of various chemical dopants:

DDQ (0.51 V) < NOBF₄ (1.34 V) < AuCl₃ (1.49 V),

it is clear that AuCl₃ has the highest positive reduction potential that makes it the strongest p-type dopant for SWCNTs (Figure 2.3.4-2). This is in good agreement with experimental observations.

Despite the fact that AuCl₃ is shown as the strongest p-dopant, it has some drawbacks, including hygroscopic effect, decrease in T_{550} , environmental stability, and high cost. Therefore, research to estimate the potential for further E_F reduction or increasing the current work function values in p-type doped SWCNT films is to be continued in order to obtain highly transparent as well as conductive SWCNT-based films.

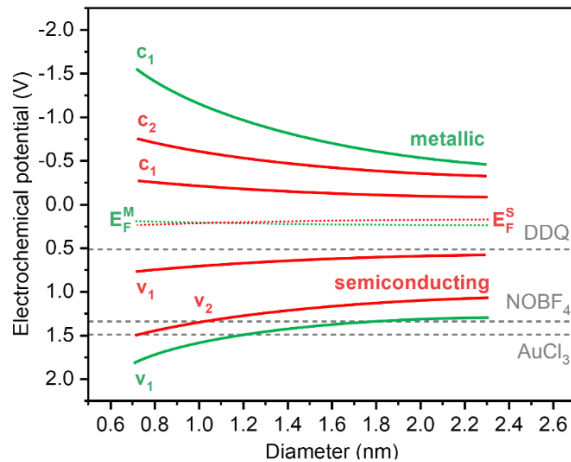


Figure 2.3.4-2. Illustration of the electrochemical potential dependence of corresponding conduction c_i and valence v_i bands of metallic (solid green) and semiconducting (solid red) nanotubes as well as related to them Fermi levels E_F^j (dotted green $j = "M"$ and red $j = "S"$, correspondingly), and p-type dopants (dashed grey) on a SWCNT diameter [40].”

4. “CHAPTER 3

3.3 Aerosol measurements. After reading this section one still does not understand what does it help for making transparent conducting films. Probably it is important to control the properties of the as grown films but it is not clear from the text of the section.”

Answer:

The discussion in the Section 3.3 was extended to provide additional necessity of this tool during synthesis and post-synthesis processes.

p.39 “Therefore, in principle and according to the discussed aerosol analysis, DMA measurements could help to reveal whether individual or bundled nanotubes are produced during aerosol CVD synthesis. Thus, a small total concentration of particles (basically less than 10^5 \#/cm^3) could be related to individual nanotubes (typical agglomeration time is less than the residence time), while a high effective diameter could be indirectly attributed to a long SWCNT length [21,54,56]. Both individuality and length are proved to be the keys parameters for transparent and conductive film development. Using DMA as an express tool of aerosol characterization, one can adjust synthesis conditions for the highest performance.”

References:

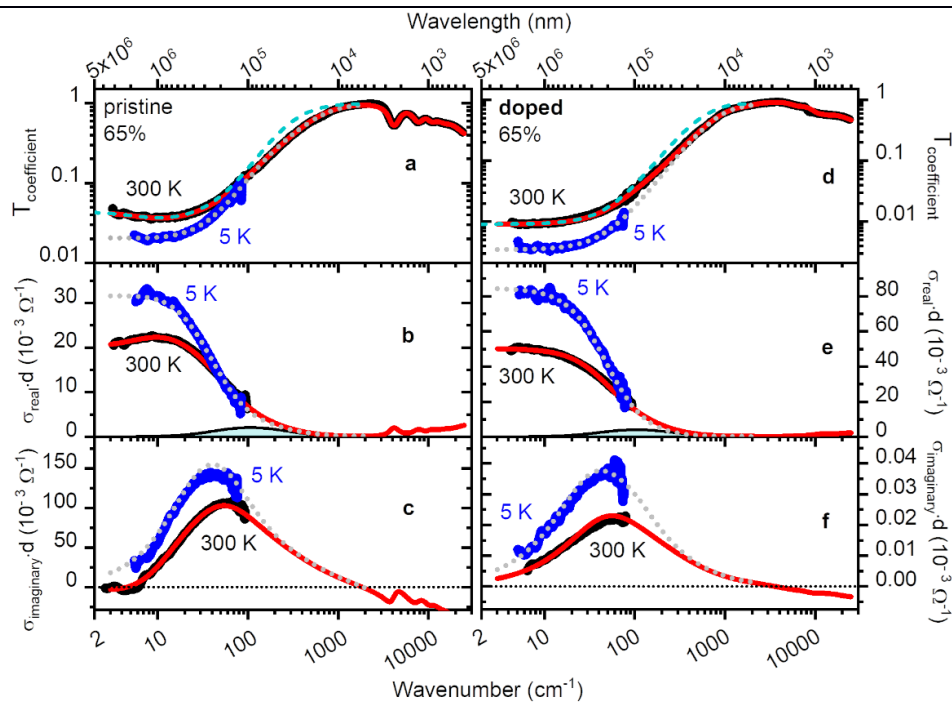
- [21] K. Mustonen, P. Laiho, A. Kaskela, T. Susi, A.G. Nasibulin, E.I. Kauppinen, Uncovering the ultimate performance of single-walled carbon nanotube films as transparent conductors, Appl. Phys. Lett. 107 (2015) 143113. doi:10.1063/1.4932942.
- [54] K. Mustonen, P. Laiho, A. Kaskela, Z. Zhu, O. Reynaud, N. Houbenov, Y. Tian, T. Susi, H. Jiang, A.G. Nasibulin, E.I. Kauppinen, Gas phase synthesis of non-bundled, small diameter single-walled carbon nanotubes with near-armchair chiralities, Appl. Phys. Lett. 107 (2015). doi:10.1063/1.4926415.
- [56] D. Hecht, L. Hu, G. Grüner, Conductivity scaling with bundle length and diameter in single walled carbon nanotube networks, Appl. Phys. Lett. 89 (2006) 2004–2007. doi:10.1063/1.2356999.

5. “CHAPTER 4 Charge carrier dynamics

Figure 4.1.1.1 there are black lines and black dots. They cannot be distinguished. The shaded area on the middle panels of Figure 4.1.1.1 can be hardly seen. Should be made as a separate figure”

Answer:

The Figure 4.1.1.1 and its capture and the corresponding text were corrected.



p.42 “Figure 4.1.1-1. Room temperature 300 K (solid black lines) and 5 K (solid blue dots) spectra of (a, d) transmission coefficient $T_{coefficient}$, (b, e) effective real $\sigma_{real} \cdot d$ and (c, f) effective imaginary $\sigma_{imaginary} \cdot d$ parts of conductances of (a, b, c) pristine and (d, e, f) doped SWCNT films ($T_{550} = 65\%$). The fitting curves for 300 K and 5 K samples are shown in solid red and dotted grey, correspondingly. The THz-sub-THz region corresponds to direct measurements on the THz pulsed TD and CW backward-wave oscillator based spectrometers. Dashed cyan lines in (a) and (d) correspond to the fit when the absorption resonances at 100 cm^{-1} in $\sigma_{real} \cdot d$ spectra (cyan-shaded areas in (b) and (e) show absorption peaks due to plasmon resonance) are not taken into account.”

p.43 “We note that in order to consistently describe the transmission and conductance spectra we had to introduce an additional term in the form of an absorption band located at $\sim 100 \text{ cm}^{-1}$. It is indicated by the cyan-shaded areas in Figure 4.1.1-1b,e and was modeled by a Lorentzian. Another feature detected in the spectra of all pristine films was a decrease of $\sigma_{real} \cdot d$ in the direction of the lowest frequencies below $\sim 10 \text{ cm}^{-1}$ at 300 K (Figure 4.1.1-1b).”

6. “With a mean-free path in our films $l = 0.1 \mu\text{m}$ (see below) we have $l/L = 0.25$ confirming that our films are practically free of impurities. The value $L = 0.4 \mu\text{m}$ this discussion is too primitive. The origin of the so called “THz peak” is still widely debated in literature. Therefore, it is important to provide extensive discussion of the matter. The fact that “average distance” between defects (or in other words plasmon confinement length) is four time the MFP should be justified more accurately. Relation between the plasmon velocity and Fermi velocity is not discussed at all”

Answer:

The extensive discussion on the mentioned matter was added to the Section 4.1.1, including the references explaining the current undestading of the THz peak nature.

p.43 “To analyze the nature of the absorption band at $\sim 100 \text{ cm}^{-1}$, we plot its spectral shapes (insets in Figure 4.1.1-2a) for all pristine and doped films ($T_{550} = 65, 75, 80, 90,$ and 95%). It can be seen that the band intensity or spectral weight (area under the $\sigma_{real} \cdot d$ curves) is larger for the doped films and quickly decreases as the T_{550} value increases (inset in Figure 4.1.1-2b). This is a strong indication that the origin of the bands should be related to the presence of delocalized charge carriers. We associate these absorption peaks with plasmon oscillations of charge carriers which are partly localized by defects, impurities and nanotube intersections. Corresponding excitations have been previously observed in numerous experiments. The amplitude of the bands is much smaller than that of the free-carrier Drude component (characterized by the $\sigma_{real} \cdot d$ value at $\sim 10 \text{ cm}^{-1}$), which makes them not so clearly expressed in these experiments. We believe that the reason is the effective screening by both delocalized carriers and only a small fraction of

localized carriers (compared to the number of delocalized carriers). The fact that the position of the bands is basically unchangeable in all studied films means that the localization distance of the carriers is determined not by the SWCNTs' ends [61], but by certain defects inside the nanotubes or their intersection. We can roughly estimate the distance between these defects as $L = V_p / (\pi \cdot \nu_p)$, where V_p is the plasmon velocity that is several times greater than the Fermi velocity [62] and ν_p is the plasma frequency. With $\nu_p = 100 \text{ cm}^{-1}$, $V_p = 4 \cdot V_F$ [62] and the Fermi velocity $V_F = 10^8 \text{ cm/s}$ [62] we obtain $L = 0.4 \text{ }\mu\text{m}$. The Fermi velocity of $V_F = 10^8 \text{ cm/s}$ is a typical value for graphene-like materials, obtained using following equation: $(\sqrt{3} \cdot a \cdot \gamma_0) / (2 \cdot \hbar)$, where a – hexagonal lattice constant, γ_0 – nearest neighbor hopping integral, which is close to 3 eV for bulk graphite. With a mean-free path (l) in our films equal to $0.1 \text{ }\mu\text{m}$ (as discussed below), we have $l/L = 0.25$ confirming that our films are practically free of impurities [62]. The value $L = 0.4 \text{ }\mu\text{m}$ correlates well with the average distance between intersections of SWCNTs, as can be seen from the atomic force microscopy studies (Figure 2a-d in Publication IV). Thus, we assume that plasmon excitations occur due to reflections of the charge carrier plasma at the SWCNT intersections. Meanwhile, a more detailed study on this matter and THz-peak nature is required for complete understanding. Also, based on the fact that broad and strong THz conductivity peak appears in both types of nanotube films (semiconducting and metallic), whose behaviors are consistent with the plasmon resonance explanation, this firmly rules out other alternative explanations such as absorption due to the curvature-induced gaps [63,64].””

References:

- [61] M. V. Shuba, A.G. Paddubskaya, A.O. Plyushch, P.P. Kuzhir, G.Y. Slepyan, S.A. Maksimenko, V.K. Ksenevich, P. Buka, D. Seliuta, I. Kasalynas, J. MacUtkovic, G. Valusis, C. Thomsen, A. Lakhtakia, Experimental evidence of localized plasmon resonance in composite materials containing single-wall carbon nanotubes, *Phys. Rev. B - Condens. Matter Mater. Phys.* (2012). doi:10.1103/PhysRevB.85.165435.
- [62] T. Nakanishi, T. Ando, Optical Response of Finite-Length Carbon Nanotubes, *J. Phys. Soc. Japan.* (2009). doi:10.1143/jpsj.78.114708.
- [63] Q. Zhang, E.H. H aroz, Z. Jin, L. Ren, X. Wang, R.S. Arvidson, A. L uttge, J. Kono, Plasmonic Nature of the Terahertz Conductivity Peak in Single-Wall Carbon Nanotubes, *Nano Lett.* 13 (2013) 5991–5996. doi:10.1021/nl403175g.
- [64] M. V. Shuba, A.G. Paddubskaya, P.P. Kuzhir, G.Y. Slepyan, D. Seliuta, I. Ka alynas, G. Valu sis, A. Lakhtakia, Effects of inclusion dimensions and p-type doping in the terahertz spectra of composite materials containing bundles of single-wall carbon nanotubes, *J. Nanophotonics.* 6 (2012) 061707. doi:10.1117/1.JNP.6.061707.

7. “Typo on page 39: “ $V_F = 107$ ” instead of “ $V_F = 10^7$ ”

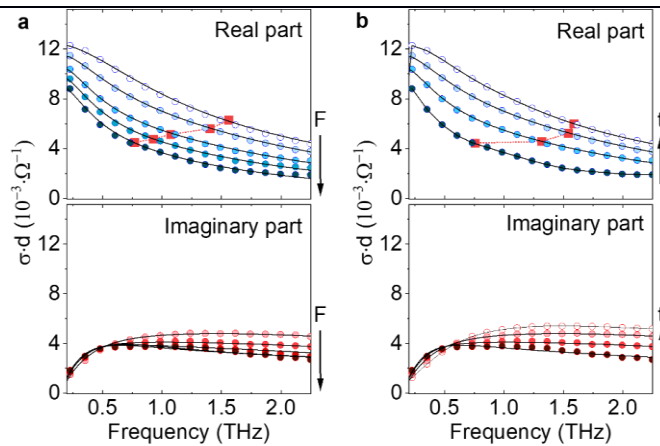
Answer:

The typo was corrected in the text on p.44.

8. “There are no green circles in the fig. 4.1.2-1. as stated in the caption. They were supposed to show the width of a peak as a function of (?) frequency as stated in the caption and discussed in the text.”

Answer:

The Figure 4.1.2-1 was corrected to match the figure caption and the text.



p.49 “Figure 4.1.2-1. (a) Equilibrium conductance (empty dots) and conductance at $t = 2 \text{ ps}$ after excitation (filled dots) of the pristine SWCNT film at laser fluences of $F = 0, 2.8, 6.95, 14.3, 26 \mu\text{J}/\text{cm}^2$. Real (blue circles) and imaginary (red circles) parts of the measured sheet conductances ($\sigma \cdot d$) are plotted. The arrow F indicates the fluence change from low to high values. Red filled squares connected by a red dotted line indicate a change in the peak width f_{HWHM} . (b) The conductance at $t = 1.8, 3.2, 5.4, 20 \text{ ps}$ after photoexcitation, for $F = 26 \mu\text{J}/\text{cm}^2$. The arrow t points from early to late times.”

p.50 “The prominent negative photoconductivity can be seen in Figure 4.1.2-1 comparing the real part of the sheet conductance ($\sigma \cdot d$) of the pristine film without excitation (empty blue circles) and 2 ps after photoexcitation at several pump fluences (filled blue circles). The observed conductivity after photoexcitation was lower in amplitude, and the enhanced suppression of $\sigma_{real}(\omega, t = 2 \text{ ps})$ (the main partial sum parameter) with the increasing fluence is evident in Figure 4.1.2-1a. A higher fluence resulted in a progressively narrowing of $\sigma_{real}(\omega, t = 2 \text{ ps})$, as can be seen for instance from the frequency f_{HWHM} at which the conductivity is half its maximum value (red filled squares in Figure 4.1.2-1). At later pump-probe delays, the conductivity was rapidly recovered back towards its equilibrium level, increasing in amplitude and broadening in width, as shown in Figure 4.1.2-1b. It should be noted that the THz peak of the conductivity is assumed to be located out of the used bandwidth as the maximum value was 0.1 THz (also, the Drude term is rising as the doping level increases and its maximum is assumed to be in GHz-region according to the previous works [63,64,69]).”

References:

- [63] Q. Zhang, E.H. Háróz, Z. Jin, L. Ren, X. Wang, R.S. Arvidson, A. Lüttge, J. Kono, Plasmonic Nature of the Terahertz Conductivity Peak in Single-Wall Carbon Nanotubes, *Nano Lett.* 13 (2013) 5991–5996. doi:10.1021/nl403175g.
- [64] M. V. Shuba, A.G. Paddubskaya, P.P. Kuzhir, G.Y. Slepyan, D. Seliuta, I. Kašalynas, G. Valušis, A. Lakhtakia, Effects of inclusion dimensions and p-type doping in the terahertz spectra of composite materials containing bundles of single-wall carbon nanotubes, *J. Nanophotonics.* 6 (2012) 061707. doi:10.1117/1.JNP.6.061707.
- [69] J.M. Marulanda, A. Srivastava, Carrier density and effective mass calculations in carbon nanotubes, in: *Phys. Status Solidi Basic Res.*, 2008. doi:10.1002/pssb.200844259.

9. “fig. 4.1.2-1. Trend of $t \Rightarrow \infty$ does not follow the trend $F \Rightarrow 0$, therefore something is wrong.”

Answer:

As it can be seen from the Figure 4.1.2-1 on p.49, we fixed the constants (fluence or time after the photoexcitation) and measured the response on a particular parameter, thus we saw the described behavior (when $t \Rightarrow \infty$, it follows the trend $F \Rightarrow 0$). Therefore the limiting/extreme case $t \Rightarrow \infty$ corresponded to the equilibrium conductance value $F \Rightarrow 0$ (for instance, in Figure 4.1.2-1b $t \Rightarrow \infty$ and in Figure 4.1.2-1a $F \Rightarrow 0$ cases).

10. “No “definition” of effective mass m^* is provided, although the term is used throughout the chapter 4. Is it the cyclotron mass p_F/v or is it $(d^2E/dp^2)^{-1}$?”

Answer:

Effective mass defined as $(d^2E/dp^2)^{-1}$ was used as it’s known to take into account the interaction of

an electron with the lattice.

11. “References to supporting information remain from copy-pasting from the paper text in the section 4.2.3.”

Answer:

Thank you for your comments. This sentence was rewritten accordingly.

p.67 “The detailed description of the experimental setup is presented in extensively discussed in Publication II. Concisely, one of the ...”

Based on the Jury Member Report from Assistant Professor Toma Susi, there have been made changes according to the following suggestions:

1. “The study on the role of solvent in the doping process also adds new physicochemical understanding, while leading to some of the highest performance films ever reported. It appears that the spray method introduced by the candidate offers good possibilities of integration with continuous production methods. The only small shortcoming of this aspect of the thesis is a comparison of the stability of various doping schemes.”

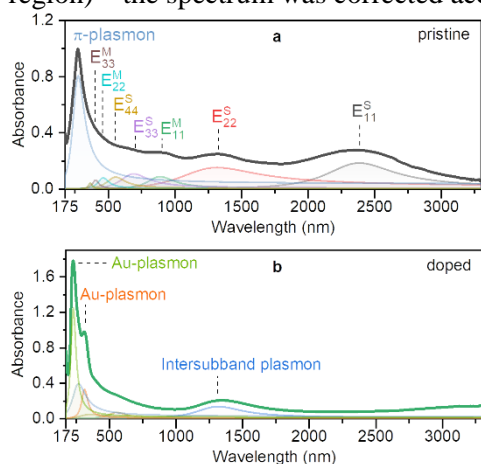
Answer:

The stability of the samples after doping by various techniques and schemes is for sure a highly required task and it would be interesting to study it in details in the upcoming works. Meanwhile, all the methods are more or less comparable (the results can almost be the same after several optimization stages during the same procedure/method – the principal stability effects remain similar according to several independent studies), while after preliminary literature analysis we found out that for practical point of view one of the best techniques is aerosol-assisted method (uniformity, fine-tuning in real time, etc.) if compared with, for instance, drop-casting and spin-coating (coffee ring effects, not completely suitable for mass production, etc.).

2. “p.19: why is there increased absorption beyond 2500 nm in the doped sample? What is the cause of the small peak at 2700 nm?”

Answer:

As it's discussed in Section 4.1.1 the measured from UV up to THz has this contributions: UV-Vis peaks $>3000\text{ cm}^{-1}$ due to **intersubband transitions vHs (Lorentz)**, IR-THz peaks $<1000\text{ cm}^{-1}$ due to **delocalized charge carriers (Drude)**, IR-THz peak at 100 cm^{-1} due to **unbound charge carriers** (energy barrier experienced by the carriers at the intersections between SWCNTs). After doping the absorbance increases, which is related to the carrier concentration increase in the film (Drude term). The peak at 2700 nm is due to depolarizer used in the scheme of UV-Vis-NIR (we didn't see the same peak during FT-IR measurements in a non-polarized mode for the same region) – the spectrum was corrected accordingly.



p.25 “Figure 2.3.2-1. Typical absorbance spectrum and the fitted peaks (after baseline subtraction) of the (a) pristine and (b) doped SWCNT films. The films are large-scale and obtained by aerosol-synthesis technique.”

3. “p.21: What does it mean that vanished vHs can be seen in Fig. 2.3.4-2? Is this the fact that the curves show no peaks? Are all the curves for doped nanotubes, and if so, what would the undoped

response look like?”

Answer:

The sentence and the section was rewritten to explain the effect concisely and in the understandable way; the correct terms were used.

p.27 “There are two main effects in the literature that govern doping [30–35]: electronegativity (in case of doping with atoms) and electrochemical potential (when doping with molecules). Both of them lead to the two main results of doping: a shift of E_F and an increase in the electron (n-doping) or hole (p-doping) carrier concentration. Additionally, the dopant may intercalate between SWCNT bundles and decrease the contact resistance between semiconducting and metallic nanotubes (reduction of the Schottky barrier height). Also, it is very important to estimate the position of E_F for a mixture of nanotubes in a film that has different DOS and consequently vHs. Therefore, simply by knowing the electronegativity or electrochemical potential (E_{NHE}^j , where j stands for the SWCNT or dopant and NHE – for normal hydrogen electrode used to experimentally determine the potential) vs. distribution relations for nanotubes and the selected dopant, the doping process can be done with the depletion of energetic states related to the vHs, which in turn will lead to the disappearance of related peak in the absorbance spectrum and change in the work function (Figure 2.3.4-1 and Figure 2.3.4-2). To relate the work function (Φ) and electrochemical potential, the work function of SWCNTs is converted to the electrochemical potential value with the two equations: $E_{NHE}^{dopant} = \Phi/e - 4.44$ (describes the reduction potential of a molecular dopant, where E_{NHE}^{dopant} is the electrode potential of the dopant to the NHE and 4.44 V stands for absolute potential of the NHE in an aqueous solution at 295.05 K) and $E_{NHE}^{SWCNT} = a/d_t + b$ (describes the redox potential of the corresponding vHs of SWCNTs, where a and b are the fitting parameters and d_t is the diameter of a nanotube). For the experimental estimation of the redox potentials of SWCNTs, electrochemistry with photoluminescence and optical absorption spectroscopy are utilized [36,37]. Figure 2.3.4-2 illustrate the dependence of an electrochemical potential of SWCNTs on the chirality/diameters, where c_i and v_i are the corresponding conduction and valence bands of metallic (solid green) and semiconducting (solid red) nanotubes, E_F^j denotes the Fermi level of metallic “M” and semiconducting “S” nanotubes. By using these plots, the adsorption dopants are selected to engineer the work function of SWCNTs. Additionally, while there are quite many stable n-type dopants [38,39] (not shown in Figure 2.3.4-2), the issue is to find a comparable p-type one.”

p.29 “Figure 2.3.4-2. Illustration of the electrochemical potential dependence of corresponding conduction c_i and valence v_i bands of metallic (solid green) and semiconducting (solid red) nanotubes as well as related to them Fermi levels E_F^j (dotted green $j = \text{“M”}$ and red $j = \text{“S”}$, correspondingly), and p-type dopants (dashed grey) on a SWCNT diameter [40].”

References:

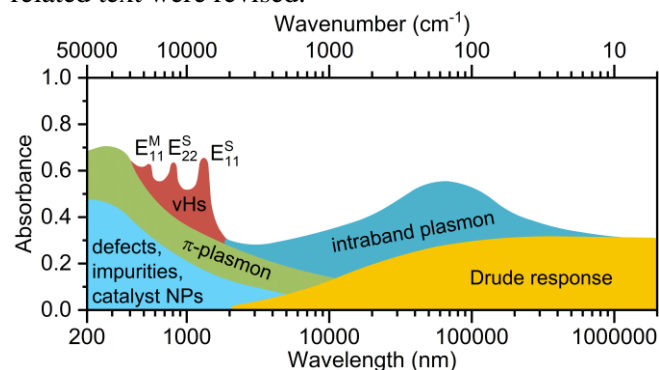
- [30] A. Murat, I. Rungger, C. Jin, S. Sanvito, U. Schwingenschlöggl, Origin of the p-Type Character of AuCl₃ Functionalized Carbon Nanotubes, *J. Phys. Chem. C*. 118 (2014) 3319–3323. doi:10.1021/jp4100153.
- [31] S.M. Kim, K.K. Kim, Y.W. Jo, M.H. Park, S.J. Chae, D.L. Duong, K.I.M.E.T. Al, Role of Anions in the AuCl₃ -Doping of Carbon Nanotubes, *ACS Nano*. (2011) 1236–1242. doi:10.1021/nn1028532.
- [32] I.H. Lee, U.J. Kim, H. Bin Son, S.-M. Yoon, F. Yao, W.J. Yu, D.L. Duong, J.-Y. Choi, J.M. Kim, E.H. Lee, Y.H. Lee, Hygroscopic Effects on AuCl₃ -Doped Carbon Nanotubes, *J. Phys. Chem. C*. 114 (2010) 11618–11622. doi:10.1021/jp1036662.
- [33] K.K. Kim, J.J. Bae, H.K. Park, S.M. Kim, H.-Z. Geng, K.A. Park, H.-J. Shin, S.-M. Yoon, A. Benayad, J.-Y. Choi, Y.H. Lee, Fermi Level Engineering of Single-Walled Carbon Nanotubes by AuCl₃ Doping, *J. Am. Chem. Soc.* 130 (2008) 12757–12761. doi:10.1021/ja8038689.
- [34] S.M. Kim, K.K. Kim, D.L. Duong, Y. Hirana, Y. Tanaka, Y. Niidome, N. Nakashima, J. Kong, Y.H. Lee, Spectroscopic determination of the electrochemical potentials of n-type doped carbon nanotubes, *J. Phys. Chem. C*. 116 (2012) 5444–5449. doi:10.1021/jp211583t.
- [35] K.K. Kim, S.M. Kim, Y.H. Lee, Chemically Conjugated Carbon Nanotubes and Graphene for Carrier Modulation, *Acc. Chem. Res.* 49 (2016) 390–399. doi:10.1021/acs.accounts.5b00441.
- [36] Y. Tanaka, Y. Hirana, Y. Niidome, K. Kato, S. Saito, N. Nakashima, Experimentally determined redox potentials of individual (n,m) single-walled carbon nanotubes, *Angew. Chemie - Int. Ed.* (2009). doi:10.1002/anie.200902468.

- [37] D. Paolucci, M.M. Franco, M. Iurlo, M. Marcaccio, M. Prato, F. Zerbetto, A. Pénicaud, F. Paolucci, Singling out the electrochemistry of individual single-walled carbon nanotubes in solution, *J. Am. Chem. Soc.* (2008). doi:10.1021/ja710625p.
- [38] S.M. Kim, J.H. Jang, K.K. Kim, H.K. Park, J.J. Bae, W.J. Yu, H. Lee, G. Kim, D.D. Loc, U.J. Kim, E.H. Lee, H.J. Shin, J.Y. Choi, Y.H. Lee, Reduction-controlled viologen in bisolvent as an environmentally stable n-type dopant for carbon nanotubes, *J. Am. Chem. Soc.* (2009). doi:10.1021/ja807480g.
- [39] B.R. Kang, W.J. Yu, K.K. Kim, H.K. Park, S.M. Kim, Y. Park, C. Kim, H.J. Shin, U. Kim, E.H. Lee, J.Y. Choi, Y.H. Lee, Restorable type conversion of carbon nanotube transistor using pyrolytically controlled antioxidizing photosynthesis coenzyme, *Adv. Funct. Mater.* (2009). doi:10.1002/adfm.200801712.
- [40] K.K. Kim, S.-M. Yoon, H.K. Park, H.-J. Shin, S.M. Kim, J.J. Bae, Y. Cui, J.M. Kim, J.-Y. Choi, Y.H. Lee, Doping strategy of carbon nanotubes with redox chemistry, *New J. Chem.* 34 (2010) 2183. doi:10.1039/c0nj00138d.

4. “p.24: Is this a real spectrum or just an illustration? The shape of the vHs contribution, especially on the higher energy side of each peak, appears strange. Or is this simply due to the logarithmic x-scale?”

Answer:

This is the illustration according to the literature search. The real spectrum can be seen, for instance, in Figure 4.1.1-1 and Figure 4.1.1-2. The Figure 3.1-1 was redrawn; the capture and related text were revised.



p.30 “Figure 3.1-1. Illustration of the typical absorbance spectrum of a pristine randomly oriented SWCNT film at room temperature revealing the main peak contributions at different wavelength regions.”

5. “p.28: The phrase “laser exposure time of 50 Hz” sounds strange. Either the unit is incorrect, or this should not be called an exposure time. Also, Raman laser power is not limited only to avoid destroying the sample, but also to avoid heating that causes changes in the response.”

Answer:

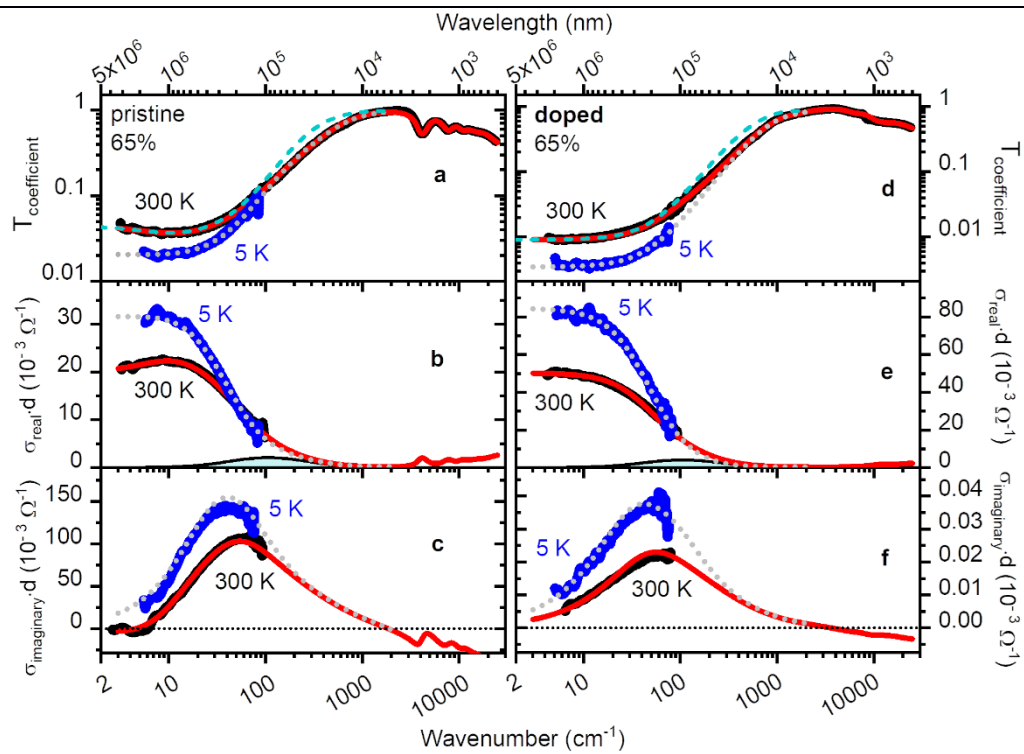
The corresponding term and unit were used. The related discussion was added to the text. In addition, I agree with the comment related with the heating.

p.35 “The laser spot was focused with long working distance 50x objective and numerical aperture of 0.50. The signal accumulation time of 20 s and laser exposure time of 0.16 s were kept constant for all the samples.”

6. “p.36: Fig. 4.1.1-1 caption “(black dots, black lines)” probably should read “(black dots, red lines)”. Also, it is not clear what “dashed lines (a) and (d)” refer to; it is hard to distinguish any such lines, should this read (c) and (f) instead? Finally, the 5 K label in (a) is poorly placed, and the presentation of the y axis scale could be unified between (a) and (d).”

Answer:

The Figure 4.1.1-1 and its capture were corrected accordingly.



p.42 “Figure 4.1.1-1. Room temperature 300 K (solid black lines) and 5 K (solid blue dots) spectra of (a, d) transmission coefficient $T_{coefficient}$, (b, e) effective real $\sigma_{real} \cdot d$ and (c, f) effective imaginary $\sigma_{imaginary} \cdot d$ parts of conductances of (a, b, c) pristine and (d, e, f) doped SWCNT films ($T_{550} = 65\%$). The fitting curves for 300 K and 5 K samples are shown in solid red and dotted grey, correspondingly. The THz-sub-THz region corresponds to direct measurements on the THz pulsed TD and CW backward-wave oscillator based spectrometers. Dashed cyan lines in (a) and (d) correspond to the fit when the absorption resonances at 100 cm^{-1} in $\sigma_{real} \cdot d$ spectra (cyan-shaded areas in (b) and (e) show absorption peaks due to plasmon resonance) are not taken into account.”

7. “p.38: What is the given Fermi velocity based on, is this from the literature? If so, reference should be given.”

Answer:

The Fermi velocity was based on a typical value for graphene-like materials as described in the corrected version of the text with the corresponding references.

p.44 “The Fermi velocity of $V_F = 10^8 \text{ cm/s}$ is a typical value for graphene-like materials, obtained using following equation: $(\sqrt{3} \cdot a \cdot \gamma_0) / (2 \cdot \hbar)$, where a – hexagonal lattice constant, γ_0 – nearest neighbor hoping integral, which is close to 3 eV for bulk graphite. With a mean-free path (l) in our films equal to $0.1 \mu\text{m}$ (as discussed below), we have $l/L = 0.25$ confirming that our films are practically free of impurities [62]. The value $L = 0.4 \mu\text{m}$ correlates well with the average distance between intersections of SWCNTs, as can be seen from the atomic force microscopy studies (Figure 2a-d in Publication IV). Thus, we assume that plasmon excitations occur due to reflections of the charge carrier plasma at the SWCNT intersections. Meanwhile, a more detailed study on this matter and THz-peak nature is required for complete understanding. Also, based on the fact that broad and strong THz conductivity peak appears in both types of nanotube films (semiconducting and metallic), whose behaviors are consistent with the plasmon resonance explanation, this firmly rules out other alternative explanations such as absorption due to the curvature-induced gaps [63,64].”

References:

- [62] T. Nakanishi, T. Ando, Optical Response of Finite-Length Carbon Nanotubes, J. Phys. Soc. Japan. (2009). doi:10.1143/jpsj.78.114708.
 [63] Q. Zhang, E.H. Hároz, Z. Jin, L. Ren, X. Wang, R.S. Arvidson, A. Lüttge, J. Kono, Plasmonic Nature of the Terahertz Conductivity Peak in Single-Wall Carbon Nanotubes, Nano Lett. 13 (2013) 5991–5996. doi:10.1021/nl403175g.

[64] M. V. Shuba, A.G. Paddubskaya, P.P. Kuzhir, G.Y. Slepian, D. Seliuta, I. Kašalynas, G. Valušis, A. Lakhtakia, Effects of inclusion dimensions and p-type doping in the terahertz spectra of composite materials containing bundles of single-wall carbon nanotubes, J. Nanophotonics. 6 (2012) 061707. doi:10.1117/1.JNP.6.061707.

8. “p.39: Is the Boltzmann constant missing from the equation? Also, it is not clear from the text how exactly were the tunnel gaps determined. Lower down on the page, it is mentioned that the effective was $0.2 m_e$, what is this based on? If literature, reference should be given.”

Answer:

p.44 “To account for the low-frequency downturn of $\sigma_{real} \cdot d$ (which is proportional to absorption), observed in pristine films, we recall that their response is determined by two contributions to the DC/AC conductivity [60,65]. One of them is connected with the intrinsic conductivity of the individual nanotube or nanotube bundles. The other is governed by the fluctuation-assisted tunneling of charge carriers through the energy barriers at the inter nanotube contacts. Therefore, the total resistivity ρ_{DC} at a given temperature T is given by:

$$\rho_{DC}(T) = \frac{1}{\sigma_{DC}(T)} = \rho_m \cdot \exp\left(-\frac{T_m}{T}\right) + \rho_t \cdot \exp\left(\frac{T_t}{T_s + T}\right),$$

where T_m (parameter related with the phonon-related part of resistance), T_t (tunneling contribution) and T_s are the temperature-related parameters, the temperature $T_m = (h \cdot \nu)/k_B$ accounts for the backscattering of the charge carriers within the individual SWCNT or nanotube bundle, the temperature T_t is related to thermal energy $k_B \cdot T_t$ which corresponds to the typical energy barrier $E_t \sim k_B \cdot T_t$ for carrier tunneling with k_B as the Boltzmann constant, the ratio T_t/T_s determines the tunneling in the absence of fluctuations and thus the conductivity $\sigma_{DC}(T \rightarrow 0)$ in the low-temperature limit, and ρ_m and ρ_t coefficients are temperature independent factors. The values of the tunnel gaps can be estimated as $1.4 \div 1.6 meV$ (corresponding to temperatures $T_t = 16 \div 18 K$ [60]) for pristine SWCNT films and as $0.2 \div 0.25 meV$ ($T_t = 2 \div 3 K$ [60]) for doped films (this estimation corresponds to the CuCl3 doped films, but we expect that it does not differ much from the films doped with AuCl3). Let $h\nu$ be the energy of electromagnetic radiation that probes the response of the film (h is the Planck’s constant). Then, for this energy that exceeds much the tunnel gap ($h \cdot \nu \gg k_B \cdot T_t$) the radiation does not “feel” the presence of a small gap, and the charge carriers respond as if they were free. In another case, $h \cdot \nu < k_B \cdot T_t$, the carriers experience an impeding tunnel gap leading to lower AC and DC conductivities. The same behavior is observed at $10 cm^{-1}$ for pristine films, where the tunnel gap energy corresponds to a frequency of $11 \div 13 cm^{-1}$. Similarly, in the spectra of doped SWCNT films measured at much higher frequencies, no signs of the tunnel gaps of $0.2 \div 0.25 meV$ (corresponding frequencies are $1.4 \div 2 cm^{-1}$) were found.”

p.46 “Having identified the Drude-like component in the response of the films it is possible to extract effective parameters of corresponding charge carriers. A typical downturn towards high frequencies in real conductance $\sigma_{real} \cdot d$ or the peak position of the imaginary conductance $\sigma_{imaginary} \cdot d$ (Figures 4.1.1-1 and 4.1.1-2) provides the carriers’ scattering rate γ which, in turn, allows to calculate: the effective mobility $\mu = e/(2 \cdot \pi \cdot m^* \cdot \gamma)$ – where e is the electron charge and $m^* = 0.2 \cdot m_e$ is its effective mass; the collision time $\tau = 1/(2 \cdot \pi \cdot \gamma)$; the mean-free path $l = \tau \cdot V_F$ (with the Fermi velocity of $V_F = 8 \cdot 10^7 cm/s$) [66]. These quantities are plotted in Figure 4.1.1-3 where it is seen that they are practically independent of the film transmittances T_{550} . As expected, the obtained values of the mobility and mean-free path are much smaller than those of individual SWCNTs ($\mu = 1,000 \div 30,000 cm^2/(V \cdot s)$ and $l = 1 \div 2 \mu m$) [67,68] due to the effect of inter nanotube contact phenomena.”

References:

[60] V.I. Tsebro, A.A. Tonkikh, D. V. Rybkovskiy, E.A. Obraztsova, E.I. Kauppinen, E.D. Obraztsova, Phonon contribution to electrical resistance of acceptor-doped single-wall carbon nanotubes assembled into transparent films, Phys. Rev. B. (2016). doi:10.1103/PhysRevB.94.245438.

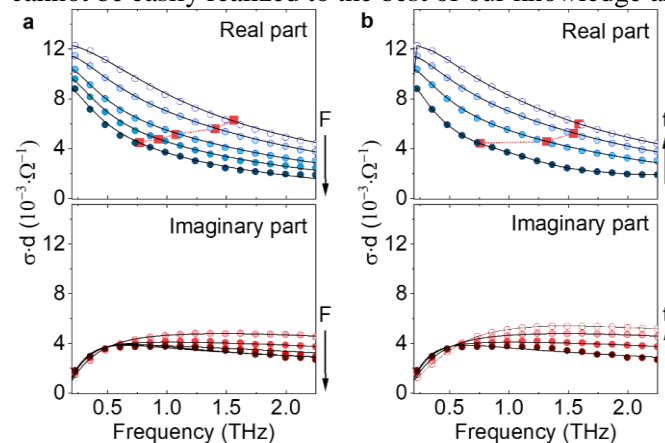
[65] A.B. Kaiser, Electronic transport properties of conducting polymers and carbon nanotubes, Reports Prog. Phys. (2001). doi:10.1088/0034-4885/64/1/201.

- [66] L.C. Venema, J.W.G. Wildöer, J.W. Janssen, S.J. Tans, H.L.J. Temminck Tuinstra, L.P. Kouwenhoven, C. Dekker, Imaging electron wave functions of quantized energy levels in carbon nanotubes, *Science* (80-.). (1999). doi:10.1126/science.283.5398.52.
- [67] J.T. Hong, D.J. Park, J.Y. Moon, S.B. Choi, J.K. Park, Farbian Rotermund, J.Y. Park, S. Lee, Y.H. Ahn, Terahertz wave applications of single-walled carbon nanotube films with high shielding effectiveness, *Appl. Phys. Express*. (2012). doi:10.1143/APEX.5.015102.
- [68] J.Y. Park, S. Rosenblatt, Y. Yaish, V. Sazonova, H. Üstünel, S. Braig, T.A. Arias, P.W. Brouwer, P.L. McEuen, Electron-phonon scattering in metallic single-walled carbon nanotubes, *Nano Lett.* (2004). doi:10.1021/nl035258c.

9. “p.43: Fig. 4.1.2-1 caption mentions “green circles connected by a black line”, but none are visible. Should the extra red filled circles in (a) and (b) top be colored green instead (and connected by a line)? What is the magnitude of the FWHM change? In the text, the word “dipper” probably should read “deeper”.”

Answer:

The mistakes were corrected and the Figure 4.1.2-1 was redrawn accordingly to the figure capture and text. The magnitude of the FWHM change can only be approximately estimated from the assumed trend to the frequency of 0 THz. The measurements of photoconductivity in this region cannot be easily realized to the best of our knowledge and literature search.



p.49 “Figure 4.1.2-1. (a) Equilibrium conductance (empty dots) and conductance at $t = 2 \text{ ps}$ after excitation (filled dots) of the pristine SWCNT film at laser fluences of $F = 0, 2.8, 6.95, 14.3, 26 \mu\text{J}/\text{cm}^2$. Real (blue circles) and imaginary (red circles) parts of the measured sheet conductances ($\sigma \cdot d$) are plotted. The arrow F indicates the fluence change from low to high values. Red filled squares connected by a red dotted line indicate a change in the peak width f_{HWHM} . (b) The conductance at $t = 1.8, 3.2, 5.4, 20 \text{ ps}$ after photoexcitation, for $F = 26 \mu\text{J}/\text{cm}^2$. The arrow t points from early to late times.”

p.50 “The prominent negative photoconductivity can be seen in Figure 4.1.2-1 comparing the real part of the sheet conductance ($\sigma \cdot d$) of the pristine film without excitation (empty blue circles) and 2 ps after photoexcitation at several pump fluences (filled blue circles). The observed conductivity after photoexcitation was lower in amplitude, and the enhanced suppression of $\sigma_{real}(\omega, t = 2 \text{ ps})$ (the main partial sum parameter) with the increasing fluence is evident in Figure 4.1.2-1a. A higher fluence resulted in a progressively narrowing of $\sigma_{real}(\omega, t = 2 \text{ ps})$, as can be seen for instance from the frequency f_{HWHM} at which the conductivity is half its maximum value (red filled squares in Figure 4.1.2-1). At later pump-probe delays, the conductivity was rapidly recovered back towards its equilibrium level, increasing in amplitude and broadening in width, as shown in Figure 4.1.2-1b. It should be noted that the THz peak of the conductivity is assumed to be located out of the used bandwidth as the maximum value was 0.1 THz (also, the Drude term is rising as the doping level increases and its maximum is assumed to be in GHz-region according to the previous works [63,64,69]).”

References:

- [63] Q. Zhang, E.H. Hároz, Z. Jin, L. Ren, X. Wang, R.S. Arvidson, A. Lüttge, J. Kono, Plasmonic Nature of the Terahertz Conductivity Peak in Single-Wall Carbon Nanotubes, *Nano Lett.* 13 (2013) 5991–5996. doi:10.1021/nl403175g.
- [64] M. V. Shuba, A.G. Paddubskaya, P.P. Kuzhir, G.Y. Slepian, D. Seliuta, I. Kašalynas, G.

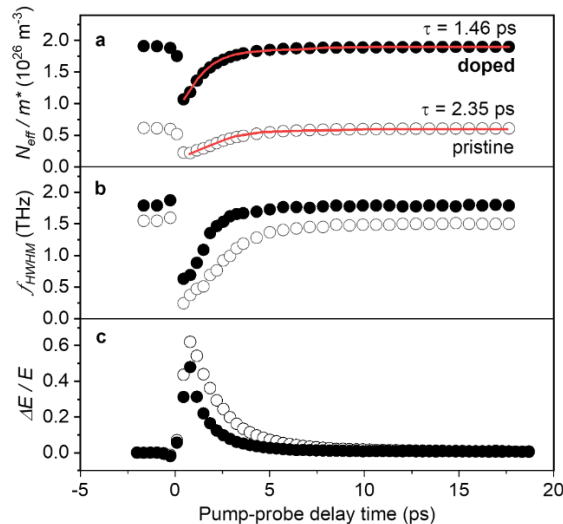
Valušis, A. Lakhtakia, Effects of inclusion dimensions and p-type doping in the terahertz spectra of composite materials containing bundles of single-wall carbon nanotubes, J. Nanophotonics. 6 (2012) 061707. doi:10.1117/1.JNP.6.061707.

[69] J.M. Marulanda, A. Srivastava, Carrier density and effective mass calculations in carbon nanotubes, in: Phys. Status Solidi Basic Res., 2008. doi:10.1002/pssb.200844259.

10. “p.44: The trion lifetime mentioned in the text needs a literature citation. Also, the mentioned solid lines in Fig. 4.1.2-2 are probably missing from the figure.”

Answer:

The trion lifetime was estimated based on previous studies [62,77], including (Nishihara, T.; Okano, M.; Yamada, Y.; Kanemitsu, Y. Review - Photophysics of Trions in Single-Walled Carbon Nanotubes. ECS J. Solid State Sci. Technol. 2017, 6, M3062). The Figure 4.1.2-2 was corrected.



p.51 “Figure 4.1.2-2. (a) The ratio of effective density of electrons to the effective mass N_{eff}/m^* vs. pump-probe delay time t for pristine (open circles) and 15 mM doped (filled circles) samples. Solid red lines illustrate fits using $N_{eff}/m^*(t) = A - B \cdot e^{-t/\tau}$, where A is the equilibrium value of N_{eff}/m^* and B is the modulation depth. (b) Frequency width f_{HWHM} of $\sigma_{real}(\omega, t)$ vs. t . (c) $\Delta E/E$ at the peak of the THz pulse vs. t .”

References:

[62] T. Nakanishi, T. Ando, Optical Response of Finite-Length Carbon Nanotubes, J. Phys. Soc. Japan. (2009). doi:10.1143/jpsj.78.114708.

[77] T. Nishihara, Y. Yamada, M. Okano, Y. Kanemitsu, Trion formation and recombination dynamics in hole-doped single-walled carbon nanotubes, Appl. Phys. Lett. (2013). doi:10.1063/1.4813014.

11. “p.47: It is unclear what the relevance of the heated Al surface experiments are for the hybrid material where the surface would consist of a nanotube network. Surely the two surfaces have very different properties?”

Answer:

The idea of this experiment was to show the possible processes happening during graphene oxide (GO) deposition. The Al substrate was used only as a model substrate allowing to distinguish the deposited GO easily (better contrast) during SEM characterization, while the deposited GO on SWCNT directly was hard to characterize precisely. At the same time, the effects of adhesion and other surface related properties were only partially taken into an account with the contact angle measurements. Therefore, a more detailed study on surface morphology, its properties etc. is still required on this matter.

12. “p.48: Reference to supplementary material seems spurious. Also, it is not clear from the text what is meant by contact angle.”

Answer:

The description of contact angle was added to the text. The required text corrections were made.

p.54 “The contact angle (or wetting angle as a measure of the wettability of a solid by a liquid) [79], θ , and the transmittance change, ΔT , were used to evaluate the degree of reduction of the GO films.”

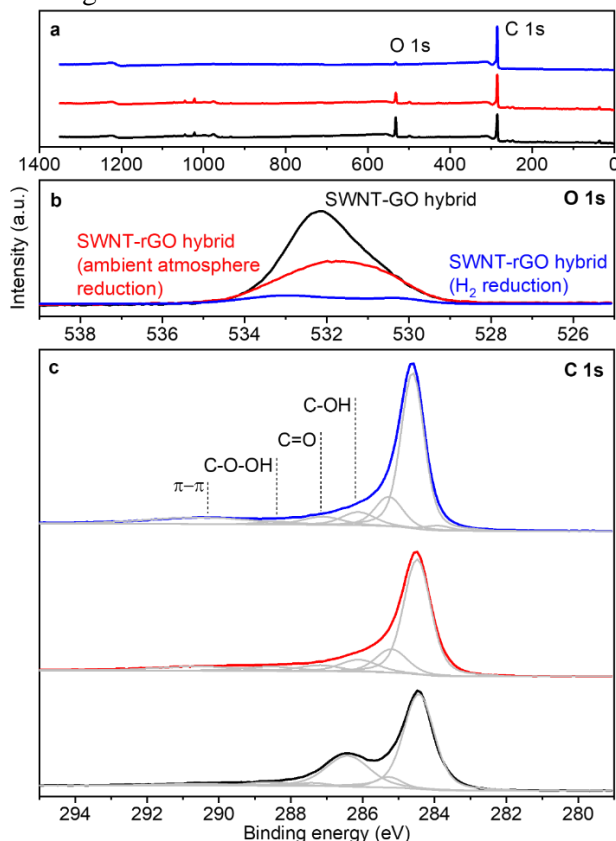
References:

[79] F. Taherian, V. Marcon, N.F.A. Van Der Vegt, F. Leroy, What is the contact angle of water on graphene?, Langmuir. (2013). doi:10.1021/la304645w.

13. “p.49: Panel (c) of Fig. 4.2.1-2 could be taller, it is very hard to see the C1s component peaks.”

Answer:

The Figure 4.2.1-2 was redrawn.



p.56 “Figure 4.2.1-2. XPS spectra of SWCNT-GO and SWCNT-rGO hybrids. (a) Comparison of XPS survey spectra of SWCNT-GO, SWCNT-rGO (reduced in ambient atmosphere) and SWCNT-rGO (reduced in H₂) hybrids, (b) O 1s XPS spectra of SWCNT-GO, SWCNT-rGO (reduced in ambient atmosphere) and SWCNT-rGO (reduced in H₂) hybrids, (c) C 1s XPS spectra of SWCNT-GO and SWCNT-rGO hybrids. The sample that was annealed in H₂ atmosphere has the lowest amount of carbon-oxygen bonds, which suggests that this method is more effective at removing oxygen-containing functional groups and reducing graphene oxide.”

14. “p.51: There seems to be a discrepancy between the equivalent resistance values given on p.48, and those shown in Fig. 4.2.1-4. Are these different samples?”

Answer:

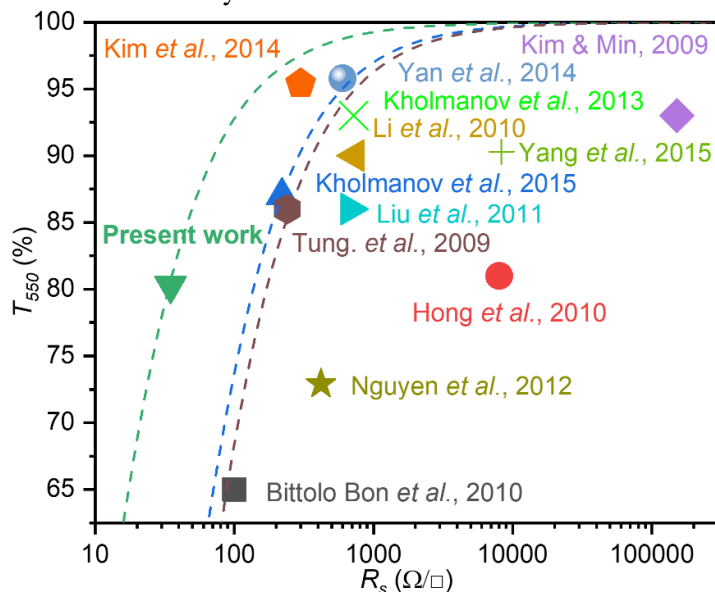
The values are for the different samples and the description in text has been updated.

p.55 “The results of the XPS studies are in agreement with the analysis of optoelectronic performance of the samples. The test samples produced by annealing in H₂ atmosphere demonstrate lower equivalent sheet resistance difference ($R_{90}^{before\ doping} - R_{90}^{after\ doping}$): their mean value is 264 Ω/□, while the samples reduced in air had a mean value of 485 Ω/□.”

15. “p.52: Is the comparison to literature data shown in Fig. 4.2.1-5 fair? Looking at the scatter plot of Fig. 4.2.1-4 (c), there appears to be no hybrid film sample that has a sheet resistance of 73 Ohm at 90% transmittance. How was this value obtained? And on p. 54, an even better value is given..?”

Answer:

The only idea was to show the R_{90} value recalculated from the obtained value of the lowest achieved R_s value for the easiness of the reader to compare with other doping methods presented later in the text. As all the other values are shown in the as-measured form and as the FoM curve is obtained from the as-measured data, the figure was redrawn accordingly and the text was corrected to clearly state that.

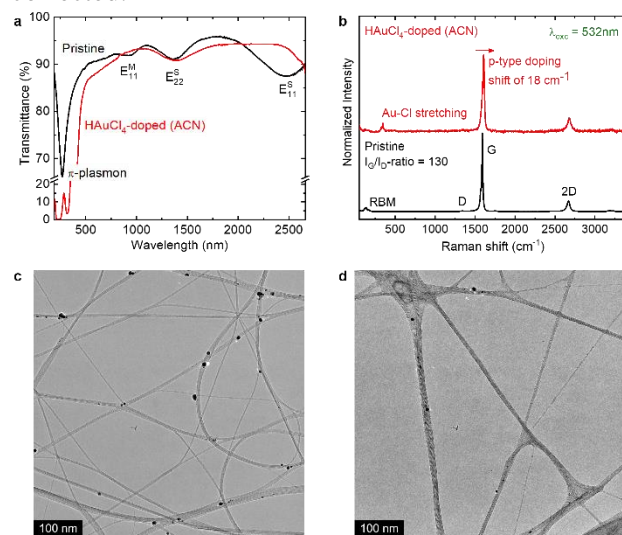


p.58 “Figure 4.2.1-5. Comparison of optoelectronic performance of SWCNT/graphene hybrids reported in the literature and in present work. Dashed lines indicate the theoretical relationship between optical transmittance at 550 nm (T_{550}) and sheet resistance (R_s) and can be used to calculate equivalent sheet resistance (R_{90}).”

16. “p.53: What is the origin of the small sharp dips at ~1300 and ~2250 nm in the H_{AuCl₄}-doped film?”

Answer:

The peaks are associated with quartz as they are present in its spectrum and were removed by simple spectrum correction based on quartz spectrum data. The description of the capture was corrected.



p.60 “Figure 4.2.2-1. Characterization of pristine and H_{AuCl₄}-doped (using acetonitrile (ACN) as a solvent) SWCNT films: (a) UV-Vis-NIR transmittance spectra of pristine (solid black) and H_{AuCl₄}-doped (dashed red) SWCNTs; (b) Raman spectra of pristine (solid black) and H_{AuCl₄}-doped (solid red) SWCNTs. TEM micrographs of (c) pristine and (d) H_{AuCl₄}-doped SWCNTs.”

17. “p.61: Mention of Supporting Information is spurious.”

Answer:

The required text corrections were made.

18. “p.63: *Using the disappearance of the vHs peaks as an indirect measure of the work function is a clever idea. However, since UPS could give this information directly, was the method cross verified? Or why were UPS measurements not performed?*”

Answer:

UPS measurements were made for pristine and several doped samples to confirm the used approach and see the correlation. The data is currently being prepared and analyzed as a separate study as additional specialization and learning was required at the time for the detailed analysis of the samples.

Based on the Jury Member Reports from *Professor Sergey Shandakov* and *Professor Alexander Okotrub*, several minor corrections on the missing abbreviations and grammatical mistakes (in “List of abbreviations and symbols”, “Chapter 2”, and “Chapter 4”,) have been made, which are similar with the previously described changes.

Moreover, some updated information and improved figures were added to the “Chapter 1” and “Chapter 4”.

Best regards and thank you once again,
Alexey